Macro Analysis of the Electro-Adsorption Process in Low Concentration NaCl Solutions for Water Desalination Applications

Carlos A. Rios Perez, Onur N. Demirer, Rebecca L. Clifton, Rachel M. Naylor and Carlos H. Hidrovo

J. Electrochem. Soc. 2013, Volume 160, Issue 3, Pages E13-E21.
doi: 10.1149/2.025303jes

Journal of The Electrochemical Society, **160** (3) E13-E21 (2013)
0013-4651/2013/160(3)/E13/9/$28.00 © The Electrochemical Society

Macro Analysis of the Electro-Adsorption Process in Low Concentration NaCl Solutions for Water Desalination Applications

Carlos A. Rios Perez, Onur N. Demirer, Rebecca L. Clifton, Rachel M. Naylor, and Carlos H. Hidrovo[z]

Mechanical Engineering Department, The University of Texas at Austin, Austin, Texas 78712, USA

Capacitive deionization (CDI) has become a very attractive desalination technology due to its capability of returning a fraction of the input energy during the regeneration of its adsorbent electrodes. As in any separation technique, analysis of the mass transfer phenomena occurring in this water treatment method is vital to evaluate and extend the performance of a desalination system. This publication proposes a novel method to estimate the net electro-adsorption rate of a CDI cell from a series of low concentration desalination experiments coupled with a one-dimensional electro-adsorption model. In the proposed methodology, a one-dimensional model is presented and two regimes are identified based on the presence or absence of a convection-diffusion layer within the bulk solution, as dictated by the electro-diffusion based Peclet number. For each of these regimes, the net adsorption flux is calculated based on the velocity at which ions are transported toward the electrodes. The proposed model is then solved, first under the assumption of an infinite electrode adsorption capacitance before relaxing this condition, and correlated against the experimental data to assess the global electro-adsorption rate. The analysis in this paper also provides unique physical insight into the macro-scale mass transfer processes that control desalination in CDI.
 [DOI: 10.1149/2.025303jes]

Manuscript submitted August 20, 2012; revised manuscript received November 5, 2012. Published January 4, 2013.

The extraction of dissolved charged particles from relatively low concentration solutions by electro-adsorption methods has gained interest in recent years. In the 1960s, the removal of ions from a solution stream by applying an electric potential to electrodes with large surface areas was initially proposed as a water desalination technique.[1–3] However, three decades passed before the development of carbon materials with a suitable high surface area allowed ionic sorption methods to become competitive with traditional techniques such as reverse osmosis and flash water desalination.[3–6] Utilizing this technology, capacitive deionization (CDI) has been proposed as a less energy intensive desalination method due to the recovery of a fraction of the input energy during a regeneration stage.

Figure 1 shows a schematic of a CDI system. During system operation, a stream of ionic solution flows between two high surface area carbon electrodes while an applied electric potential draws the ions out of the bulk solution. Adsorption of ions on the electrodes' surfaces decreases the salt concentration of the outlet solution until the saturation of the electrodes necessitates the regeneration of the system. This may be performed by either applying a second electric potential of inverse polarity or by short-circuiting the electrodes.[7] In this regeneration stage, the previously adsorbed ions are expelled into the effluent stream enabling the recovery of a fraction of the input energy. This paper focuses on the analysis of the ion extraction process prior to the regeneration of the electrodes.

Several available publications provide a general understanding of the fundamental physics behind adsorption processes in electrochemical systems. Early models of the ionic adsorption process for a porous electrode used the species conservation and Nernst-Planck equations, while assuming a steady polarization or a capacitive adsorption of ions at the solution-electrode interface.[1,8] Recent modifications to these models include the use of Poisson's equation, the consideration of the electrical double layer structure on the ionic adsorption,[9–11] and the transient non-linear adsorption response to the applied electric potential.[12,13]

Despite the above-mentioned publications, the body of literature lacks a methodology to estimate the net adsorption rate of a CDI system. General models of adsorption processes in electrochemical systems commonly focus on the interactions between the electrode matrix and the solution within the pores and not on the transport of ions in the bulk solution.[1,8,12–14] More specifically published papers on CDI assume an ideally stirred solution within a unit cell[9] or approximate important parameters (such as Stern capacitance, a transport coefficient, or a chemical attraction energy) by best fitting the temporal variation of the outlet solution concentration obtained from the compilation of a full desalination-regeneration cycle.[9–11,15] This procedure however, might provide misleading estimates because the temporal variation of outlet solution conductivity is sensitive to a diverse range of variables such as the inclusion of remnant ions from previous desalination cycles during regeneration,[16,17] the state of the electrodes,[18,19] and the sensitivity of the conductivity probes employed. Additionally, there is a large sensitivity of the outlet conductivity profile to the solution flow rate, as this paper will show.

This paper presents a one-dimensional mass conservation analysis of the electro-adsorption process within the desalination cell under two electro-adsorption regimes and two different electrode saturation conditions. Initially, the electro-adsorption process was modeled based on the extension of the mass transport mechanisms within the CDI cell as in a fully developed and developing convective diffusive layer regimes. Then, two electrode saturation scenarios were considered: an infinite and finite electrode adsorption capacity. The infinite adsorption capacitance scenario assumes that the effects of ion accumulation within the electrode are minimal on the global electro-adsorption rate. Building from this analysis, saturation effects resulting from ion accumulation in the electrodes are then considered, which affect the electro-adsorption rate within the cell in space and time. The increased complexity of this model required the implementation of a numerical algorithm to fully characterize the operating conditions.

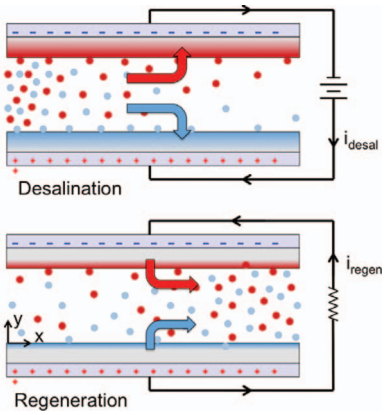

Figure 1. Capacitive deionization system. Schematic of a desalination (top) and regeneration (bottom) processes in a capacitive deionization cell.

[z]E-mail: hidrovo@mail.utexas.edu

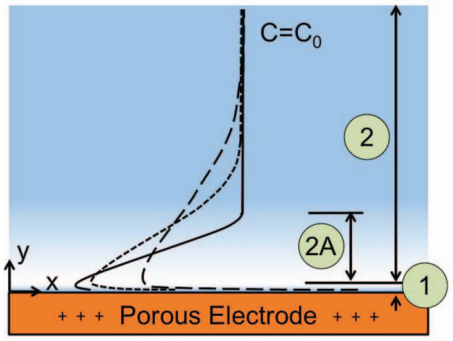

Figure 2. Schematic of the concentration variation within capacitive deionization cell. Representation of the three distinctive mass transfer regions: (1) electrode-solution interface and (2) bulk solution. The sub region (2A) convective-diffusive layer is also presented.

Background

After applying an electric potential between the electrodes of a CDI cell, the creation of concentration and electro-static potential gradients across the desalination cell drive a net flow of ions toward their respective counter electrodes. The dynamics of the electro-adsorption process have been studied previously for flat and porous electrode in a stagnant solution.[12,13] From this research, three distinctive regions (shown in Fig. 2) can be identified during the desalination process. The electrode matrix-solution interface (Region 1) is where ions are adsorbed and consists of the electrical double layer; over time, the ion adsorption will decrease due to the shielding of the electric potential by the ions in the electrodes. Next to this interface, occupying the rest of the space between electrodes, there is a bulk concentration region (Region 2) characterized by its electro-neutrality. Within this region, a sub-region (Sub-region 2A) commonly known as the convective-diffusive layer[12,20] can be identified where mass transfer effects are important.

Upon the application of the electric potential (initially acting across the entire thickness of the electrode), the selective transport of dissolved ions in different directions produces a gradient of concentrations between the electrodes. Conversely, the developed gradient of concentrations also affects the electric potential distribution producing a combined transport mechanism driven by an electric potential and a molar concentration gradient. These two transport mechanisms will act together until the electrical double layer is fully developed, and the applied electric potential is completely shielded. After this point, only molar concentration diffusion drives further variations of the ionic concentration profile.

The rate at which ions are drawn from the bulk solution varies as concentration changes in the convective-diffusive layer region. Following the application of the electric potential, the counter ion concentration at the edge of the convective-diffusive layer (in the vicinity of the electrode-solution interface) significantly decreases as ions are adsorbed. The concentration in this depleted sub-region would later increase as the ionic adsorption continues at the electrode-solution interface and saturation effects become important. This variation in the concentration gradient between the electrode solution interface and the bulk solution decreases the net rate of ionic extraction from the bulk solution due to the smaller molar concentration diffusion.

In here it is assumed that the molar ionic adsorption rate in one electrode is identical in the other, except for the difference in charge polarity. This assumption is reasonable in the bulk dilute solution when there are only two ionic species of equal charge number present (Na^+ and Cl^- for example), and the difference in mass and ionic radius effects are neglected. Consequently, the molar concentration of each ion is equal to the salt concentration in the bulk solution (quasi-neutral solution). The exception to this is the electrode-solution interface (where the electrical double layer is formed), which retains a net charge from ion accumulation meaning that electro-neutrality is not conserved.[20] The analysis of this region, however, is outside the scope of this publication.

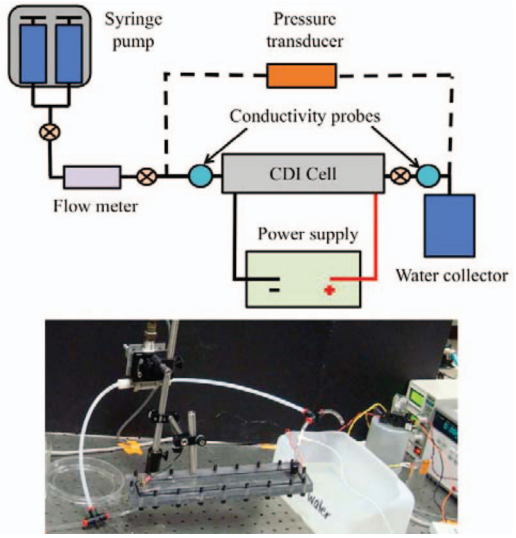

Figure 3. Experimental set-up. Schematic and picture of the capacitive deionization experimental set-up at the Multi-scale Thermal Fluids Laboratory.

Experimental Set-Up and Procedure

A laboratory-scale CDI system was designed and operated in the Multiscale Thermal Fluids Laboratory at The University of Texas at Austin. The hydraulic circuit of this system consists of a constant flow rate syringe pump, Harvard Apparatus PHD-2000, in line with an Omega FLR-1601A-V2 flowmeter, a desalination cell, two eDAQ Flow-Thru ET908 conductivity probes located at the cell inlet and outlet, an outflow reservoir, and one Omega PX409-001DWUV differential pressure transducer to measure the pressure drop across the cell. The CDI cell itself incorporates two pieces of 2.54 × 25.4 cm high-surface carbon paper Grade II (600 $m^2 \cdot g^{-1}$) from Marketech International each of which is in contact with two highly conductive titanium electrodes. A polymer mesh of 2 mm thickness separates the two pieces of carbon paper allowing the flow of the electrolyte solution between them. This mesh also firmly secures the contact of each carbon paper piece with its respective titanium electrode by pressing one against the other when the CDI cell is assembled. The external electric potential is supplied by an Agilent E3647A power supply, which also measured the electric current applied during desalination. Figure 3 shows a picture of the desalination cell and a schematic of the complete system.

The work presented here focuses on the treatment of dilute solutions (<8.556 $mol \cdot m^{-3}$ or <0.5 $mg \cdot cm^{-3}$) in an effort to analyze separately the adsorption process of ions from the electrode saturation effects. Therefore, the results obtained from the analysis of dilute solutions can be extended to industrial scale systems where the available electrode area is considerably larger and the transience before saturation might involve a significant percentage of the operation time.

During the experiments performed for this work, dilute solutions of 0.428, 0.856, and 1.283 $mol \cdot m^{-3}$ (0.025, 0.050, and 0.075 $mg \cdot cm^{-3}$ respectively) were flowed through the desalination cell at a predetermined rate until the inlet and outlet conductivity measurements were stable. Once these readings were steady, an external electrical potential of 1.0 V was applied between the electrodes. Some time after the application of this electric potential, the outlet solution conductivity decreases monotonically down to a minimum value where it would remain constant until electrode saturation effects are significant. The minimum conductivity achieved would be recorded separately as it will be used later to determine the averaged adsorption rates. As the saturation of the electrode becomes significant, the outlet solution

ionic concentration would increase back to its original value. After this point, the application of the electric potential is terminated. It is important to note that when analyzing the collected data, the time between the electric potential application and the decrease in outlet solution conductivity needs to be corrected to take into account the delay cause by the tubing volume between the desalination cell outlet and the conductivity probe.

The following section presents and briefly discusses the results of various experiments conducted following the procedure described above for different flow rates (from 0.05 to 170 $cm^3 \cdot min^{-1}$). A more exhaustive analysis of the results requires the development of a model (section *Modelling*). Following the introduction of this model, analytical and numerical solutions will be obtained and later compared to the experimental CDI performance (section *Model Solutions and Analysis*).

Experimental Results

A set of desalination experiments using solutions of 0.428, 0.856, and 1.283 $mol \cdot m^{-3}$ (0.025, 0.050, and 0.075 $mg \cdot cm^{-3}$ respectively) were conducted at various flow rates following the procedure outlined in the previous section. Figure 4 shows the time variation of the solution concentrations at low and intermediate flow rates. In this figure the solution concentration and time were normalized by the inlet solution concentration, C_0 $\{mol \cdot m^{-3}\}$, and convective time, t_{conv} $\{s\}$, respectively. The convective time represents the time that a particle would take to flow through the cell and is calculated by the ratio of cell volume to solution flow rate.

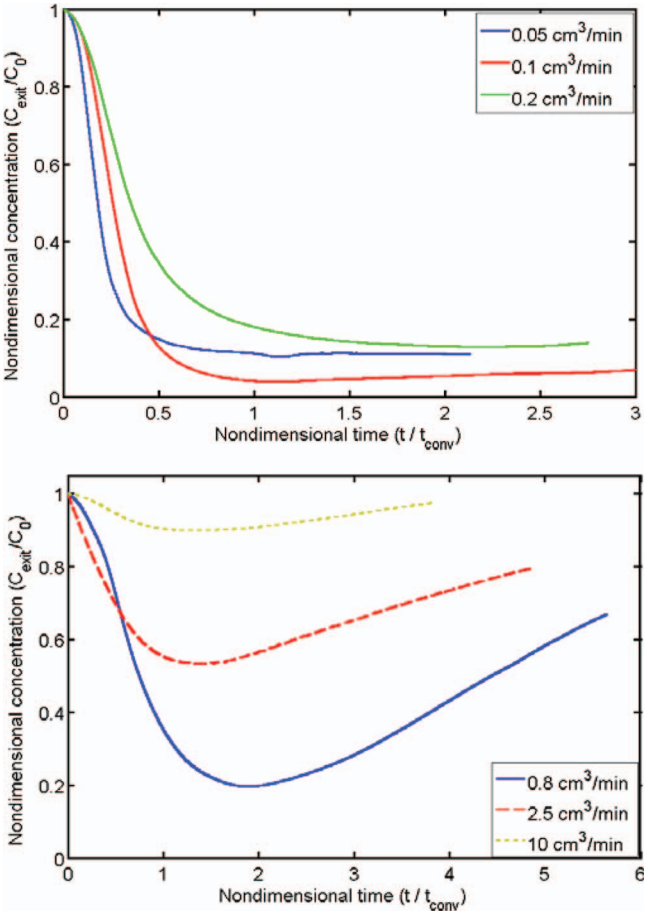

Figure 4. Experimental results: Variation of the concentration of a 1.283 $mol \cdot m^{-3}$. The solution concentration and time are standardized using the inlet concentration and convective time (time for an ion to pass through the cell) respectively for: (Top) 0.05, 0.1 and 0.2 $cm^3 \cdot min^{-1}$ showing a steady minimum concentration, (Bottom) 0.8, 2.5, and 10.0 $cm^3 \cdot min^{-1}$ showing saturation effects as concentrations increase.

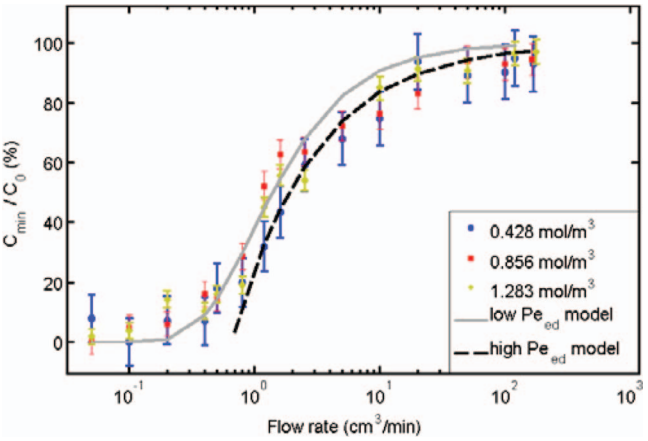

Figure 5. Variation of the minimum outlet to inlet concentration ratio and analytical solutions of the proposed model. Comparison of experimental and analytical solutions for high and low Pe_{ed} regimes for 0.428, 0.856 and 1.283 $mol \cdot m^{-3}$.

The quasi-steady minimum concentration (evident at low flow rates as shown in Fig. 4a) validates the use of dilute solutions to analyze the adsorption process by neglecting the electrode saturation effects. Conversely, by comparing Figs. 4a and 4b, it can be noted that at increasing flow rates the transition to saturation effects becomes more evident because minimum concentration does not remain constant for a significant time. This is caused by the larger amount of ions introduced in the cell per unit time as the solution flow rate increases. For each experiment, the minimum ratio of outlet and inlet solution concentrations was recorded and listed in Table I and shown in Fig. 5. The results obtained show high flow rate sensitivity, and a non-intuitive concentration independent behavior of the minimum ratio between the outlet and inlet solution concentrations in this type of systems (an approximation of CDI flow-through cell with infinite adsorption capacitance or those treating low concentration solutions).

For the error analysis, the procedure outlined by Figliola and Beasley[21] was applied to the solution flow rate as well as the outlet to inlet concentration ratios. The error in the flow rate, δQ, was determined considering the uncertainties in the input of the syringe diameter when setting the pump, δd (0.1 mm), as well as the pump displacement velocity accuracy, δp, (1% from the manufacturer catalog). Subsequently, the variance estimated for the flow rate was 1.1%. For the concentration values, the sources of uncertainty considered were the errors inherent to the calibration of the conductivity probes and the accuracy of the probe itself, which were propagated to find the error in $C_{bulk\text{-}exit}/C_0$ estimations.

The following section presents a one-dimensional model of the electro-adsorption process within a CDI cell operating at two distinct mass transfer regimes: developing and fully developed convective-diffusive layer regimes. This model was developed to predict the performance of the CDI cell and provide a better insight into the transport mechanisms in this system. Later, in section *Model Solutions and Analysis*, the solutions of this model are presented, first under the assumption of an infinite adsorption capacitance, and later relaxing this supposition. Finally, also in section *Model Solutions and Analysis*, a novel methodology to estimate the net rate of adsorption based on experimental results is introduced and the transient performance of a CDI lab-scale cell is compared between experiments and simulations.

Modeling

In a flow-by CDI cell, the bulk advection of ions in the flow direction would compete with their transport toward the electrodes. As mentioned before, mass transfer toward the electrodes is most

significant in the convective-diffusive layer. This section presents a general model of a one-dimensional electro-adsorption process of a CDI cell for two different regimes of this layer: fully developed and developing. First, in subsection *One dimensional adsorption model*, the general Nernst-Planck equation is simplified for an electro-neutral solution and a large mass Peclet number, Pe_m, scenario. Then, in subsection *Fully developed and developing convective-diffusive layer regimes*, the average net molar flux of ions is modeled independently for fully developed and developing convective-diffusive layer regimes. Finally, subsection *Developing and fully developed convective diffusive layer criterion* introduces an electro-diffusion based Peclet number, Pe_{ed}, to resolve the dominant ionic transport mechanism within the bulk solution and serve as a criterion to determine the development of the convective diffusive layer.

One dimensional adsorption model.— A general analysis of the transport of charged particles in a dilute solution, influenced by concentration and electric potential gradients, can be performed using the conservation of species and Nernst-Planck equations:

$$\frac{\partial C_i}{\partial t} = -\nabla(-\upsilon_i z_i F C_i \nabla\phi - D_i \nabla C_i + uCi) + R_i, \quad [1]$$

where C_i is the molar concentration of the ionic species i $\{\text{mol}\cdot\text{m}^{-3}\}$, υ_i is the mobility of the ionic species i $\{\text{mol}\cdot\text{s}\cdot\text{kg}^{-1}\}$, z_i is the charge number of species i, F is the Faraday's constant (9.65×10^{-4} $\text{C}\cdot\text{mol}^{-1}$), ϕ is the electrostatic potential $\{\text{V}\}$, D_i is the molar diffusivity of the ionic species $i\{\text{m}^2\cdot\text{s}^{-1}\}$, u is the bulk fluid velocity at the location of interest $\{\text{m}\cdot\text{s}^{-1}\}$, and R_i is the volumetric species i production rate $\{\text{mol}\cdot\text{s}^{-1}\}$.

Under the assumption of electro-neutrality, i.e. considering that no net charge exists in the region under analysis, the net flux of ions driven by electric potential and concentration gradients, $-\nabla(-\upsilon_i F C_i \nabla\phi - D_i \nabla C_i)$, can be combined and expressed as a concentration gradient transport phenomenon represented by: $D_{eff}\nabla^2 C_i$, where D_{eff} is the effective diffusion coefficient which includes both, the electric potential driven motion and the molar diffusion effects.[20] Therefore, the transport of charged particles in a dilute electro-neutral binary electrolyte can be described by:

$$\frac{\partial C_i}{\partial t} = \nabla_{eff}\nabla^2 C_i - u\nabla C_i + R_i, \quad [2]$$

where, as in Eq. 1, C_i is the molar concentration of the ionic species i $\{\text{mol}\cdot\text{m}^{-3}\}$, D_{eff} is the effective diffusion coefficient $\{\text{m}^2\cdot\text{s}^{-1}\}$ introduced in the previous paragraph, and u is the bulk fluid velocity $\{\text{m}\cdot\text{s}^{-1}\}$.

To further simplify the analysis of a desalination cell as a one-dimensional model, a hydraulic fully developed scenario is assumed and the concept of bulk solution concentration is introduced. Also, any electric potential gradient as well as molecular diffusion of ions in the flow direction (X-direction in Figs. 1 and 2) are assumed negligible. The bulk solution concentration of the ionic species i, $C_{bulk\text{-}i}$, for a hydraulically fully developed flow is defined in a similar manner to bulk temperature[22,23] as:

$$C_{bulk-i}(x) = \frac{w}{Q}\int_0^H C_i(x,y)U(y)dy, \quad [3]$$

where w is the width of the desalination cell $\{\text{m}\}$, Q is the solution flow rate within the cell, $\{\text{m}^3\cdot\text{s}^{-1}\}$, H is the separation between electrodes $\{\text{m}\}$, and $U(y)$ is the velocity distribution of the solution across the cell (Y-direction in Figs. 1 and 2) $\{\text{m}\cdot\text{s}^{-1}\}$.

Neglecting the electric potential gradients in the flow direction can be intuitive as it is expected that the electric potential gradients normal to the flow are significantly larger due to the small separation between electrodes. Thus, the transport of ions in the X-direction (flow direction) would be primarily driven by the bulk flow advection and the molar diffusion. The relative importance of one or another of these mechanisms can be compared by evaluating the mass transfer Peclet number, Pe_m, defined as:

$$Pe_m = \frac{Q\cdot L}{w\cdot H\cdot D_i}, \quad [4]$$

where L $\{\text{cm}\}$ is the desalination cell length. For all the experiments conducted in this paper, Pe_m was larger than 1×10^4 (for a $D_{NaCl} = 1.24\times10^{-5}$ $\text{cm}\cdot\text{s}^{-1}$[20]), and consequently, advection dominated the transports of ions in the flow direction.

The transport of ionic species within the CDI cell, previously described by Eq. 2, can now be modeled as a one-dimensional species conservation equation as:

$$\frac{\partial C_{bulk-i}}{\partial t} = \frac{-Q}{H\cdot w}\cdot\frac{\partial C_{bulk-i}}{\partial x} - \frac{j_{ads-i}}{H}. \quad [5]$$

Here, $j_{ads\text{-}i}$ represents net molar flux of ionic species i $\{\text{mol}\cdot\text{cm}^{-2}\cdot\text{s}^{-1}\}$ adsorbed from the bulk solution and is expected to vary along the cell. Note that in this expression, the transport of ions within the electro-neutral bulk solution (in the X-direction and represented in the first term of the right hand side) has been separated from the net adsorption flux of charged particles toward the electrodes (in the Y-direction and represented by the second term of the right hand side). In other words, the model is one-dimensional with the bulk concentration only being dependent on the X-direction, with the cross-cell transport in the Y-direction being treated as a production (destruction in this case) rate term.

Building upon this one-dimensional model, in the next section the adsorption flux, j_{ads}, is modeled for two distinctive convective-diffusive layer regimes.

Fully developed and developing convective-diffusive layer regimes.— In a flow-through CDI cell, the bulk advection of ions in the flow direction would compete with their transport toward the electrodes. As mentioned before, the sub-region within the bulk solution where mass transfer toward the electrodes is significant is called the convective-diffusive layer and has been used to model the electro-adsorption of ions in this type of system.[9,12,24–26] The analysis of this convective diffusive layer can be performed at the two regimes shown in Fig. 6: fully developed and developing.

Fully developed convective-diffusive layer.—When the convective-diffusive layer is fully developed, the transport of ions within the bulk solution toward their respective counter ions is significant and uniform throughout the whole bulk solution. Subsequently, as ions at the edge of the bulk solution region are electro-adsorbed onto the electrodes, the ions between the electrodes would "rapidly rearrange" significantly decreasing the concentration gradients normal to the flow direction. Therefore, the net average molar flux of ions from the bulk solution at a specific location along the cell is modeled for this scenario as:

$$j_{ads}(x) = C_{bulk}(x)\cdot v_{ads}, \quad [6]$$

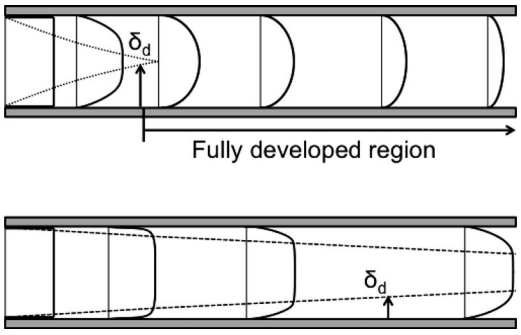

Figure 6. Schematic of the fully developed and developing convective-diffusive layers. Representation of the ionic concentration profiles at low (top) and high (bottom) Pe_{ed} regimes.

where v_{ads} is the net adsorption velocity or the rate at which ions would migrate toward the electrode $\{m \cdot s^{-1}\}$. Similarly to the diffusion coefficient and electro-mobility, v_{ads} is assumed to be concentration independent for dilute solutions and consequently is constant along the cell.

Developing convective-diffusive layer.—Mass adsorption effects within a desalination cell at large flow rates were assumed to be confined to the developing convective-diffusive layer. The rationale behind this approach is that at large flow rates, ions in the flow core would not be able to significantly migrate toward the electrical double layers as they are carried downstream out of the cell. Therefore, the region where mass transfer effects are important is confined next to the electrode-solution interfaces, and only the small portion of charged particles near the electrodes would be adsorbed. The Nernst Layer approximation is a common approximation made to model this limited region where mass transfer is important. This approximation assumes a linear gradient of concentrations across this film as shown in Fig. 6. Under the Nernst Layer approximation, the net adsorption flux of an impermeable electrodes cell can be described by:[20]

$$j_{ads}(x) = D_{eff} \frac{C_0 - C_{edge}}{\delta_D(x)}. \quad [7]$$

Here j_{ads} is the net molar flux at which ions are adsorbed from the bulk solution $\{mol \cdot m^{-2} \cdot s^{-1}\}$, C_O is the inlet solution molar concentration $\{mol \cdot m^{-3}\}$ and which remains constant out of the Nernst layer, C_{edge} is the molar concentration at the bottom of the Nernst layer (next to the solution-electrode interface) $\{mol \cdot m^{-3}\}$, δ_D is the Nernst Layer thickness $\{m\}$, and x is the distance from the cell entrance to the section of interest in the flow direction $\{m\}$. Note that for the analysis of a system with infinite adsorption capacitance electrodes, C_{edge} is zero as the accumulation of charge at the electrode-solution interface and its immediate surroundings is negligible.

In Eq. 7, the effective diffusion coefficient and the X-dependent Nernst layer thickness can be grouped together to define the net adsorption velocity, v_{ads}, in a developing convective-diffusive layer as:

$$v_{ads}(x) = \frac{D_{eff}}{\delta_D(x)}. \quad [8]$$

As a first approximation, the growth of the Nernst layer thickness in a CDI cell with infinite adsorption capacitance is assumed to be similar to the one in a channel flow with soluble walls (case analyzed by Probstein[20]):

$$\frac{\delta_D(x)}{x} = 1.289 \left(\frac{H}{x}\right)^{2/3} \left(\frac{D_{eff}}{\overline{U} \cdot H}\right)^{1/3}. \quad [9]$$

Here, $\overline{U}$ is the average flow velocity $\{cm \cdot s^{-1}\}$ and H is the channel thickness $\{cm\}$. Note that the Nernst Layer thins as the flow rate increases.

Introducing this relationship into Eq. 8, and replacing the average flow velocity by the ratio of the solution flow rate, Q, and the CDI cell cross sectional area, $w \cdot H$, reveals the dependence of the X-dependent net adsorption velocity, v_{ads}, on the solution flow rate:

$$v_{ads}(x) = 0.776 \left(\frac{D_{eff}}{H}\right)^{2/3} \left(\frac{Q}{x \cdot w}\right)^{1/3} \quad [10]$$

It must be stressed that in a developing convective-diffusive layer, the net adsorption velocity, v_{ads}, is X-dependent as it aims to account for the transport of ions through a thin, growing, and limited region (Nernst layer) where concentration gradients are significant. On the other hand, in a fully developed convective-diffusive layer regime, this velocity represents the net transport of ions across the entire bulk solution and is constant along the cell. It is therefore expected that v_{ads} would be larger in a developing than in a fully developed regime due to the larger concentration gradients across the thin Nernst layer typical of developing convective-diffusive layers.

Returning to the net adsorption flux for developing convective-diffusive layers, assuming infinite adsorption capacitance electrodes and introducing Eq. 10 into Eq. 7 when $C_{edge} = 0$, the net molar adsorption flux can be expressed as:

$$j_{ads}(x) = 0.776 \cdot C_0 \cdot \left(\frac{D_{eff}}{H}\right)^{2/3} \left(\frac{Q}{w \cdot x}\right)^{1/3}. \quad [11]$$

This concludes the model of the X-dependent net molar adsorption flux, j_{ads}, at developing and fully developed regimes. Next, we introduce a criterion to determine whether the convective system under analysis is in a developing or fully developed regime.

Developing and fully developed convective diffusive layer criterion.— Estimating the thickness of the convective-diffusive layer at the exit of the cell (using Eq. 9), and comparing it with the separation between electrodes, would verify the suitability of a developing or fully developed convective-diffusive layer assumption. Looking at Eq. 9, the electro-diffusion Peclet number, Pe_{ed}, may be defined as:

$$Pe_{ed} = \frac{\overline{U} \cdot H}{D_{eff}}. \quad [12]$$

This parameter can determine whether or not the convective-diffusive layer is fully developed. Developing regimes would have a large Pe_{ed} (as they are characterized by a large average solution velocity) while fully developed regimes would present a low Pe_{ed}. However, the use of this dimensionless number requires prior knowledge of D_{eff} or its estimation from experimental data. As an alternative to determining the effective diffusivity, it is proposed here to use the ratio of the net adsorption velocity, v_{ads}, to the average bulk velocity, $\overline{U}$, as the characteristic parameter to evaluate the development of the convective-diffusive layer. From Eqs. 8 and 9, the ratio of the convective convective-diffusive layer thickness to electrode separation is:

$$\frac{\delta_D(x)}{H} = 1.463 \cdot \left(\frac{v_{ads}(x) \cdot x}{\overline{U} \cdot H}\right)^{1/2}. \quad [13]$$

This expression was derived from the Nernst layer approximation of a thin and developing convective-diffusive layer in a channel with soluble walls.[20] Consequently, it is expected that a constant average net adsorption velocity (defined in the *Appendix*), $\overline{v_{ads}}$, can substitute the X-dependent net adsorption velocity without losing much accuracy in the approximation.

The next section (*Model Solutions and Analysis*) presents the solutions of the model on each regime for two distinctive cases: when the electrode saturation effects are neglected and a quasi-steady condition is assumed, and when these two conditions are relaxed.

Model Solutions and Analysis

This section presents the solutions of the model introduced above for the low and high Pe_{ed} regimes corresponding to fully developed and developing convective-diffusive layer. First, in subsection *Infinite adsorption capacitance (steady state) solution*, a steady and infinite electrode adsorption capacitance scenario is assumed to obtain analytical solutions for Eq. 5. Then, the net adsorption velocity at a fully developed and developing convective-diffusive regimes are estimated comparing the solutions obtained and experimental results of the minimum exit to inlet concentration ratios in subsection *Net adsorption velocity estimation at low and high* Pe_{ed}. Finally, the steady and infinite adsorption capacitance assumptions are relaxed, and a finite difference algorithm is used to solve Eq. 5 numerically to estimate the time behavior of the outlet solution concentration in subsection *Finite adsorption capacitance (transient) solution.*

Infinite adsorption capacitance (steady state) solution.— When steady and infinite adsorption capacitances are assumed, it is possible to analytically solve the one-dimensional model presented in Eq. 5, 6, and 11.

Low Pe_{ed} regime.—Initial analysis considered a fully developed convective-diffusive layer (or low Pe_{ed}) regime where convection of the ions in the flow direction dominates their movement within the cell. Substituting Eq. 6 into Eq. 5 and solving the resulting differential equation, the ratio of the bulk concentration of the outlet and inlet concentrations is:

$$\frac{C_{bulk-exit}}{C_0} = \exp\left(\frac{-v_{ads} \cdot w \cdot L}{Q}\right). \quad [14]$$

High Pe_{ed} regime.—In a developing convective-diffusive layer regime, the electro-adsorption toward the electrodes is comparable to the advection of ions by the bulk solution. Assuming steady state conditions, and substituting the net average molar flux of ions from Eq. 11 into the one-dimensional model (Eq. 5), the bulk solution concentration at the exit of the desalination cell is given by:

$$\frac{C_{bulk-exit}}{C_o} = 1 - 1.164 \cdot \left(\frac{D_{eff} \cdot w \cdot L}{H \cdot Q}\right)^{2/3}. \quad [15]$$

After introducing the average net adsorption velocity ($\overline{v_{ads}}$) defined in the *Appendix*, Eqs. 11 and 15 can be rewritten as:

$$j_{ads}(x) = \frac{2}{3} \cdot \overline{v_{ads-ref}} \cdot C_0 \left(\frac{L \cdot Q}{x \cdot Q_{ref}}\right)^{1/3}, \quad [16]$$

$$\frac{C_{bulk-exit}}{C_o} = 1 - \left(\frac{w \cdot L \cdot \overline{v_{ads-ref}}}{Q^{2/3} \cdot Q_{ref}^{1/3}}\right), \quad [17]$$

where $\overline{v_{ads-ref}}$ $\{m \cdot s^{-1}\}$ is the average net adsorption velocity at reference flow rate Q_{ref} $\{m^3 \cdot s^{-1}\}$. The *Appendix* presents a more detailed derivation of Eqs. 16 and 17 for the interested reader.

Equations 14 and 17 show the suitability of estimating the reference average net adsorption velocity, $\overline{v_{ads-ref}}$, and the net adsorption velocity, v_{ads}, (at high and low Pe_{ed} regimes respectively) by evaluating the ratio of outlet to inlet concentrations of dilute solutions. The procedure to follow to determine these two velocities is outlined in the following subsection.

Net adsorption velocity estimation at low and high Pe_{ed}.— This subsection outlines the procedure followed to determine the net adsorption velocity, v_{ads} (at a low Pe_{ed} regime), and the reference average net adsorption velocity, $\overline{v_{ads-ref}}$ (at a high Pe_{ed} regime), from an iteration process that minimizes the root mean square error between the results from Eqs. 14 and 17, and the experiments described in section *Experimental Set-Up and Procedure*. The minimization of the mean squared error was employed as an optimization parameter to estimate the velocities that best describe the experiments.

Low Pe_{ed} regime.—For a fully developed convective-diffusive layer regime, a value of v_{ads} is assumed and introduced into Eq. 14 to calculate the ratio $C_{bulk\text{-}exit}/C_0$ at various flow rates within a pre-selected range of values. The ratio of concentrations obtained is then compared with their corresponding experimental values for each flow rate and the root-mean-squared error between the predicted ratios and those measured at different flow rates in the preselected range. This procedure is repeated for different values of v_{ads} until the root-mean-squared error is minimized. The net adsorption velocity assigned to the system at a low Pe_{ed} regime would be the one employed to obtain this minimum.

At this point, a question might arise about the range of flow rates picked for this estimation and whether or not they correspond to a fully develop or low Pe_{ed} regime. In this publication, this range was also methodically varied. As a first estimation, the lowest four flow rates at which experiments were conducted were analyzed. Further variations in the range of flow rates used would include the addition of immediately higher flow rate. On each range, the net adsorption velocity was optimized, and a minimum root-mean-square error was obtained. The final flow rate range and v_{ads} selected would represent the lowest root-mean-squared error.

Following the procedure described above, the optimum net adsorption velocity obtained was 2.50×10^{-4} cm $\cdot$ s^{-1} with a root-mean-squared error of 10.63. This estimation was obtained in a flow rate range from 0.05 to 0.5 cm$^3 \cdot$ min^{-1} (Pe_{ed}<70). From Eq. 15, the Nernst layer becomes fully developed ($\delta_D = H/2$) at 0.29 and 2.9 cm from the cell entrance at 0.05 to 0.5 cm$^3 \cdot$ min^{-1} respectively, i.e. more than 88.6% of the cell length would be fully developed. This validates the initial assumption of a fully developed convective-diffusive layer (low Pe_{ed})

High Pe_{ed} regime.—In a high Pe_{ed} regime the reference average net adsorption velocity is determined by comparing the ratios of the outlet and inlet solution concentrations with the analytical solution of the proposed one-dimensional model given in Eq. 17. This time however, two parameters would need to be optimized in this analysis: the reference average net-adsorption velocity, $\overline{v_{ads-ref}}$, and its respective flow rate, Q_{ref}. The modified procedure also starts by selecting a range of high flow rates where the optimization will be performed. The lowest flow rate in this chosen range is designated as Q_{ref} and the optimization algorithm is applied to vary $\overline{v_{ads-ref}}$ in the analytical solution (Eq. 17) until the root-mean-squared error with the experimental data is minimized. As in the low Pe_{ed} regime analysis, the flow rate range where this optimization process was conducted is also changed. As a first estimation, the highest four flow rates at which experiments were conducted were analyzed. Additional increment in this range would include the immediately lower flow rate. The optimal $\overline{v_{ads-ref}}$ was determined at the range with the lowest root-mean-squared error.

The reference average net adsorption velocity, $\overline{v_{ads-ref}}$, was estimated as 4.70×10^{-4} cm $\cdot$ s^{-1} with a root-mean-squared error of 4.53 for flow rates between 10 and 168 cm$^3 \cdot$ min^{-1} ($Pe_{ed} > 1.1 \times 10^3$). The reference flow rate for this high Pe_{ed} regime was 10 cm$^3 \cdot$ min^{-1}. In this developing convective-diffusive layer range, the Nernst layer thickness grows up to 0.09 to 0.02 cm respectively (45% and 10% of the distance between electrodes) validating the initial assumption of a developing convective-diffusive layer.

Figure 5 shows the agreement between the ratios of outlet to inlet solution concentrations obtained experimentally as well as the analytical solutions for low and high Pe_{ed} regimes (Eqs. 14 and 17 respectively) for the net adsorption velocities estimated in this section. At flow rates lower than 0.5 cm$^3 \cdot$ min^{-1} the desalination percentages predicted by the low Pe_{ed} model falls within the confidence interval in most of the experiments while the high Pe_{ed} model predicts negative values. This situation is inversed between 10 to 100 cm$^3 \cdot$ min^{-1} where the low Pe_{ed} model overestimates the desalination percentages while the high Pe_{ed} model successfully estimates them within the experimental variance. Last, at very large flow rates (120 and 170 cm$^3 \cdot$ min^{-1}), both models predictions fall within the experimental data confidence interval. Under these high flow rates and Pe_{ed} conditions, the variation in the outlet solution concentration is smaller than the confidence range of the experiments. However, the high Pe_{ed} model predictions are closer to the mean of the data in this range as compared to the low Pe_{ed} model.

Attempting to quantify the percentage error between the model predictions and experimental results at low flow rates (low Pe_{ed} regime) would be misleading since the estimated experimental error is larger than or close to both, the nominal measurement and the model prediction. For example, at 0.05 cm$^3 \cdot$ min^{-1}, the low Pe_{ed} model prediction and experimental measurement at 1.283 mol $\cdot$ m^3 were 3.0×10^{-9} and 0.018 ± 0.027 respectively. For flow rates $\geq$ 10 cm$^3 \cdot$ min^{-1} (high Pe_{ed} regime), the average error between the model predictions and experiments was 3.38%.

This concludes the analysis of the one-dimensional model and its analytical solutions under the steady and infinite adsorption capacitance assumptions. In the following subsection, these two conditions are relaxed.

Finite adsorption capacitance (transient) solution.— In general, the relaxation of the infinite capacitance assumption requires the

introduction of a changing net average molar adsorption flux as a function of amount of ions adsorbed and, consequently, the ionic concentration at the solution-electrode interface, $C_{interface}$ $\{\text{mol}\cdot\text{cm}^{-3}\}$.[12,13] As more ions are pulled from the bulk solution and accumulated at the electrode-solution interface, the electrical double layer would be developed and the applied electric potential would be shielded at the solution-electrode interface decreasing the transport of ions driven by the weakened electric field within the solution. Parallel to this, the accumulation of ions in the electrode solution interface will affect the concentration difference between this interface and the bulk solution further decreasing the net average flux of ions from the bulk solution to the electrode.

This section introduces the accumulation of ions and the finite adsorption capacitance effects in the model of j_{ads} for low Pe_{ed} and high Pe_{ed} regimes by decreasing this net flux. This adjustment was made by introducing the time-dependent factor ($1\text{-}N_{interface}/N_{max}$) in the net molar adsorption flux models (Eqs. 6 and 11). Here $N_{interface}$ and N_{max} represent the amount of ions accumulated in the electrode-solution interface, and the maximum amount of ions that can be adsorbed respectively. The introduction of this time dependent coefficient makes necessary the use of numerical methods to solve the one-dimensional model presented in Eq. 5 for fully developed and developing convective-diffusive layer regimes.

Before proceeding to compare the transient behavior of the concentration obtained experimentally with the numerical model predictions, it must be noted that the conductivity probe has a delayed response to highly transient concentration changes such as those encountered at the beginning of the desalination cycle. These initial effects have been accounted for in the numerical solutions by the addition of a delayed response similar to that of the probe.

Low Pe_{ed} regime.—In a fully developed convective-diffusive layer regime with finite adsorption capacitance, the one-dimensional model introduced in Eqs. 5 and 6 can be discretized using a first order finite difference algorithm forward in time (explicit) and backward in space as:

$$\frac{C^{t+1}_{bulk-j}-C^{t}_{bulk-j}}{\Delta t}=\frac{Q}{w\cdot H}\left(\frac{C^{t}_{bulk-(j-1)}-C^{t}_{bulk-j}}{\Delta x}\right)-C^{t}_{bulk-j}\cdot v^{0}_{ads}\left(1-\frac{N^{t}_{interface-j}}{N_{max}}\right), \quad [18]$$

where Δx $\{\text{m}\}$ is the differential element length of the uniformly discretized cell (in the flow direction), Δt $\{\text{s}\}$ the duration of each time step of the simulation, v^{o}_{ads} $\{\text{m}\cdot\text{s}^{-1}\}$ is the net adsorption velocity assuming an infinite adsorption capacitance in the electrodes, $N_{interface\text{-}j}$ $\{\text{mol}\}$ is the accumulated amount of ions absorbed in the element j, and $N_{max\text{-}j}$ $\{\text{mol}\}$ is finite capacity of ions that can be adsorbed in the element j. For this manuscript, $N_{max\text{-}j}$ was obtained for every flow rate and concentration modeled by dividing the experimental total number of moles adsorbed by the total number of elements in which the cell was numerically discretized). The subscripts and superscripts in Eq. 18 denote the discrete location in the flow direction and the discrete time instants respectively.

Figure 7 shows the agreement between the experimental results and the solution of Eq. 18 when $v^{o}_{ads}=2.50\times10^{-4}$ $\text{cm}\cdot\text{s}^{-1}$ (estimated on the infinite adsorption capacitance and low Pe_{ed} model) to predict the dimensionless concentration variation of a 1.283 $\text{mol}\cdot\text{m}^{-3}$ (0.075 $\text{mg}\cdot\text{cm}^{-3}$) solution at three different flow rates (0.1, 0.4, and 1.6 $\text{cm}^3\cdot\text{min}^{-1}$).

High Pe_{ed} regime.—Similarly to the low Pe_{ed} regime, the one-dimensional adsorption model (Eq. 5) and the net molar adsorption flux model (Eq. 16) can be combined and numerically discretized using a finite difference algorithm forward in time (explicit) and backward in space as:

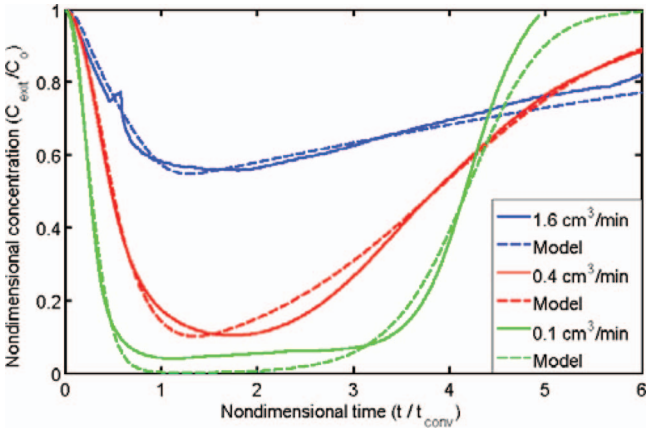

Figure 7. Numerical solution of the one-dimensional model at low Pe_{ed}. Comparison of the experimental (solid line) and predicted (dashed line) concentration with time for a 1.283 $\text{mol}\cdot\text{m}^{-3}$ at 0.1, 0.6, and 1.6 $\text{cm3}\cdot\text{min}^{-1}$.

$$\frac{C^{t+1}_{bulk-j}-C^{t}_{bulk-j}}{\Delta t}=\frac{Q}{w\cdot H}\left(\frac{C^{t}_{bulk-(j-1)}-C^{t}_{bulk-j}}{\Delta x}\right)-\overline{v_{ads-ref}}\cdot\left(\frac{2}{3}\right)\left(\frac{C_0}{H}\right)\times\left(\frac{Q\cdot L}{Q_{ref}\cdot(j\cdot\Delta x)}\right)^{1/3}\left(1-\frac{N^{t}_{interface-j}}{N_{max}}\right) \quad [19]$$

where $\overline{v_{ads-ref}}$ and Q_{ref} are the reference average net adsorption velocity and its respective reference flow rate estimated above under the infinite adsorption capacitance assumption (subsection *Net adsorption velocity estimation at low and high Pe_{ed}*; *High Pe_{ed} regime*). Also, as in the low Pe_{ed} regime, $N_{interface\text{-}j}$ and $N_{max\text{-}j}$ are the accumulated amount of ions absorbed and maximum capacity of ions that can be adsorbed in the element j respectively.

Figure 8 shows the agreement between the experimental results and the solution of Eq. 19 when $\overline{v_{ads-ref}}=4.70\times10^{-4}$ $\text{cm}\cdot\text{s}^{-1}$ and $Q_{ref}=10$ $\text{cm}^3\cdot\text{min}^{-1}$ are used to estimate the dimensionless outlet solution concentration variation of a 1.283 $\text{mol}\cdot\text{m}^{-3}$ (0.075 $\text{mg}\cdot\text{cm}^{-3}$) solution at 10, 20, and 50 $\text{cm}^3\cdot\text{min}^{-1}$

Equations 18 and 19 were solved using a numerical model developed in MATLAB. The model proved to be time and space steps independent at $\Delta x=0.5$ cm and $\Delta t=0.1$ s with an averaged variation lower than 0.2% when these two quantities were reduced in half.

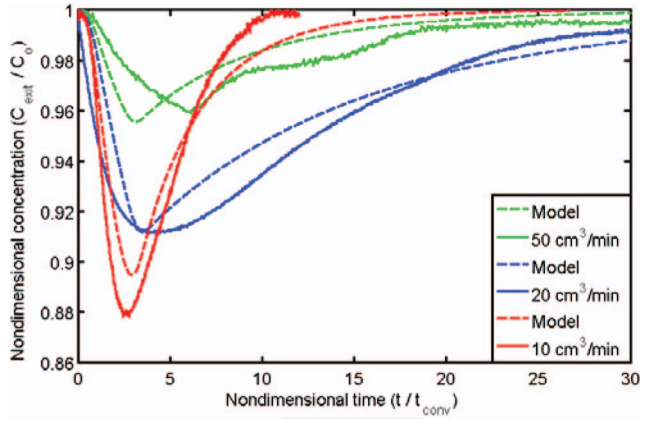

Figure 8. Numerical solution of the one-dimensional model at high Pe_{ed}. Comparison of the experimental (solid line) and predicted (dashed line) concentration with time for a 1.283 $\text{mol}\cdot\text{m}^{-3}$ at 10, 20, and 50 $\text{cm}^3\cdot\text{min}^{-1}$.

Although the scheme used in this work is a first order approximation (the error of the model will be reduced proportional to the reduction of the discretized element size), the computational cost and error obtained using the above mentioned discretization parameters remained low. Future change to a two- or three-dimensional model might require the use of a higher order scheme to improve the accuracy of the model.

Conclusions

In this paper, a novel methodology to determine the ionic adsorption velocity in a CDI cell was introduced. First, a one-dimensional model for a CDI cell was presented and a simplified model of the net molar adsorption flux, j_{ads}, was introduced for high and low Pe_{ed} regimes providing physical insight into the difference in these operating conditions. In this regard, the net adsorption velocity was defined for both regimes, and an optimization procedure to estimate this velocity from experimental data was proposed.

The analytical solutions obtained by assuming steady state and negligible saturation effects were used to determine the net adsorption velocity at low and high Pe_{ed} regimes. Experimental results showed that the time concentration profiles do not remain constant at the minimum values for intermediate and high flow rates as was expected for infinite adsorption capacity electrodes. However, the agreement between the analytical and experimental minimum outlet to inlet concentration ratios suggests that the error from this assumption would not be detrimental for very dilute solutions. Therefore, the analysis of low concentration solutions allows the determination of the characteristic ionic transport velocities following the methodology of this publication.

The net adsorption velocity was estimated for two different flow rate ranges. Calculating the thickness of the region where mass transfer effects are significant validated the adequacy of the flow rates selected to describe the low and high Pe_{ed} regimes ($Pe_{ed} < 70$ and $Pe_{ed} > 1100$ respectively). The reference average net adsorption velocity estimated at the large Pe_{ed} (4.70×10^{-4} cm $\cdot$ s^{-1}) was larger than the one determined at a low Pe_{ed} regime (2.50×10^{-4} cm $\cdot$ s^{-1}). This difference appears to arise due to the thinner Nernst layer encountered at higher flow rates, which causes a larger concentration gradient and a net molar flux.

The ionic transport velocities estimated were input into a numerical model, which relaxes the steady state and negligible saturation assumptions and accurately mimics the experimental results. It was seen that for low concentrations, electrical double layer shielding could be modeled as a decrease in the molar adsorption flux, j_{ads}, which in this model is linearly related to the electrode ionic concentration. This conclusion is supported by the test results at low and high Pe_{ed} regimes in Figs. 7 and 8.

The models accurately predicted the minimum outlet to inlet solution concentration ratios, as well as the concentration time variation concentration shown in Figs. 5, 7, and 8, suggesting that the low and high Pe_{ed} models developed are applicable when the solution flow rates are <1 and >10 cm^3 $\cdot$ min^{-1} respectively ($Pe_{ed} < 100$ and $Pe_{ed} > 1000$ accordingly). It is expected that at intermediate flow rates (1–10 cm^3 $\cdot$ min^{-1}) the low and high Pe_{ed} models bound the behavior of the system, which is indeed the case as depicted in Fig. 5. Future work will test the model and methodology proposed in this paper with brackish concentrations to validate the transport velocities and electrical double layer shielding models.

Among the sources of error between the models and experimental data are: the use of the Nernst layer approximation (linearization of the concentration profile within the convective-diffusive layer), the one-dimensional simplification of the model, the inherent numerical error of a first order approximation, and the accuracy and resolution of the instrumentation (conductivity sensors, flowmeter, and syringe pump).

The methodology to determine the net adsorption velocity and the molar adsorption flux model developed in this paper provide both temporal and spatial information about the concentration profiles inside the CDI cell. Therefore, it might be used as a tool to evaluate the performance of existing CDI systems and possibly to design and scale new systems.

Acknowledgments

The authors of this paper thank Brian Carroll, Collier Miers, and Mara Sweeney for their help on the development of the experimental set-up. The authors would also like to thank Dr. Mark Deinert for his support of this project.

Appendix - Determination of the average adsorption velocity (High Pe_{ed} regimes)

In this appendix, we show in detail the definition of the average net adsorption velocity and the derivation of the adsorption flux in terms of this introduced variable. We start our discussion with Eq. 10 from the paper:

$$v_{ads}(x) = 0.776 \left(\frac{D_{eff}}{H}\right)^{2/3} \left(\frac{Q}{x \cdot w}\right)^{1/3}. \quad [A.1]$$

where v_{ads} {cm $\cdot$ s^{-1}} is the net adsorption velocity at hi Pe_{ed} regimes, D_{eff} is the effective diffusion coefficient, {cm^2 $\cdot$ s^{-1}}, Q is the flow rate {cm^3 $\cdot$ s^{-1}}, H is the channel thickness {cm}, w is the channel width {cm}, and x is the distance from the cell entrance to the section of interest in the flow direction {cm}.Under the infinite electrode adsorption capacity assumption, the adsorption flux can be estimated as:

$$j_{ads}(x) = C_O \cdot v_{ads}(x) \quad [A.2]$$

where C_O is the inlet solution concentration {mol $\cdot$ m^{-3}}, which remains constant out of the convective diffusive layer along the total length of the cell, L {cm}. The average net adsorption velocity, $\overline{v_{ads}}$, is defined to make the adsorption flux constant and X-independent while conserving the total rate of ions adsorbed along the whole CDI cell:

$$C_O \cdot \overline{v_{ads}} \cdot w \cdot L = \int_L C_O \cdot v_{ads}(x) \cdot w \cdot dx \quad [A.3]$$

Substituting Eq. A.1 into A.3, and simplifying:

$$\overline{v_{ads}} = 0.776 \left(\frac{3}{2}\right) \left(\frac{D_{eff}}{H}\right)^{2/3} \left(\frac{Q}{L \cdot w}\right)^{1/3} \quad [A.4]$$

Assuming a constant flow rate Q, and effective diffusivity D_{eff}, the average net adsorption velocity, $\overline{v_{ads}}$, can be presented as a function of a reference average net adsorption velocity, and the flow rate at which it occurs:

$$\overline{v_{ads}} = \overline{v_{ads-ref}} \left(\frac{Q}{Q_{ref}}\right)^{1/3} \quad [A.5]$$

Finally, combining Eqs. A.1, A.4, and A.5, the X-dependent adsorption velocity can be expressed as:

$$v_{ads} = \overline{v_{ads-ref}} \left(\frac{Q \cdot L}{Q_{ref} \cdot x}\right)^{1/3} \left(\frac{2}{3}\right) \quad [A.6]$$

Equation A.6 is the relation used to derive Eqs. 16 and 19 in this manuscript.

List of Symbols

Latin letters

z_i	Charge number of species i
u	Bulk fluid velocity at the location of interest {cm $\cdot$ s^{-1}}
w	Width of the desalination cell {cm}
j_{ads}	Net molar adsorption flux {mol $\cdot$ cm^{-2} $\cdot$ s^{-1}}
x	Distance from the cell entrance to the section of interest in the flow direction {cm}
v_{ads}	Net adsorption velocity {cm $\cdot$ s^{-1}}
C_i	Molar concentration of the ionic species i {mol $\cdot$ cm^{-3}}
F	Farady's constant (9.65×10^{-4} C $\cdot$ mol^{-1}}
D_i	Molar diffusivity of species i {cm^2 $\cdot$ s^{-1}}
R_i	Volumetric species i production rate {mol $\cdot$ cm^{-3} $\cdot$ s^{-1}}
D_{eff}	Effective diffusion coefficient {cm^2 $\cdot$ s^{-1}}
$C_{bulk\text{-}i}$	Bulk solution concentration of the ionic species i {mol $\cdot$ cm^{-3}}
$C_{bulk\text{-}exit}$	Bulk solution concentration at the exit of the cell {mol $\cdot$ cm^{-3}}

Q	Solution flow rate within the cell $\{cm^3 \cdot s^{-1}\}$
U	Velocity the solution across the cell $\{cm \cdot s^{-1}\}$
H	Separation between electrodes $\{cm\}$
L	Desalination cell length $\{cm\}$
Pe_m	Mass transfer Peclet number
C_O	Inlet solution molar concentration $\{mol \cdot cm^{-3}\}$
C_{edge}	Molar concentration at the bottom of the Nernst layer $\{mol \cdot cm^{-3}\}$
Re_x	Reynold's number
Sc	Schimdt number
Q_{ref}	Reference flow rate$\{cm^3 \cdot s^{-1}\}$
Pe_{ed}	Electro-diffusion Peclet number
$N_{interface}$	Amount of ions accumulated in the electrode-solution interface $\{mol\}$
N_{max}	Maximum number of ions that can be adsorbed in the electrode $\{mol\}$
$\overline{v_{ads}}$	Average net adsorption velocity $\{cm \cdot s^{-1}\}$
$\overline{v_{ads-ref}}$	Average reference net adsorption velocity $\{cm \cdot s^{-1}\}$
$\overline{U}$	Average flow velocity $\{cm \cdot s^{-1}\}$
Δx	Length of a discretized element in a finite difference algorithm $\{cm\}$
Δt	Time step in a finite difference algorithm $\{s\}$

Greek letters

υ_i	Mobility of the ionic species i $\{mol \cdot s \cdot kg^{-1}\}$
ϕ	Electrostatic potential $\{V\}$
δ_D	Nernst Layer thickness $\{cm\}$

References

1. A. M. Johnson and J. Newman, *Journal of The Electrochemical Society*, **118**, 510 (1971).
2. Y. Oren and A. Soffer, *Journal of Applied Electrochemistry*, **13**, 473 (1983).
3. M. A. Anderson, A. L. Cudero, and J. Palma, *Electrochimica Acta*, **55**, 3845 (2010).
4. R. W. Pekala, J. C. Farmer, C. T. Alviso, T. D. Tran, S. T. Mayer, J. M. Miller, and B. Dunn, *Journal of Non-Crystalline Solids*, **225**, 74 (1998).
5. J. Wang, L. Angnes, H. Tobias, R. A. Roesner, K. C. Hong, R. S. Glass, F. M. Kong, and R. W. Pekala, *Analytical Chemistry*, **65**, 2300 (1993).
6. J. Farmer, D. Fix, G. Mack, R. Pekala, and J. Poco, *Journal of Applied Electrochemistry*, **26**, 1007 (1996).
7. K. Dermentzis and K. Ouzounis, *Electrochimica Acta*, **53**, 7123 (2008).
8. J. S. Newman and C. W. Tobias, *Journal of The Electrochemical Society*, **109**, 1183 (1962).
9. P. M. Biesheuvel, B. van Limpt, and A. van der Wal, *The Journal of Physical Chemistry C*, **113**, 5636 (2009).
10. B. G. Jeon and H. C. No, *Desalination*, **288**, 66 (2012).
11. R. Zhao, P. M. Biesheuvel, H. Miedema, H. Bruning, and A. van der Wal, *The Journal of Physical Chemistry Letters*, **1**, 205 (2009).
12. P. M. Biesheuvel and M. Z. Bazant, *Phys. Rev. E*, **81**, 031502 (2010).
13. M. Z. Bazant, K. Thornton, and A. Ajdari, *Phys. Rev. E*, **70**, 021506 (2004).
14. M. van Soestbergen, P. M. Biesheuvel, and M. Z. Bazant, *Phys. Rev. E*, **81**, 021503 (2010).
15. S. Porada, L. Weinstein, R. Dash, A. van der Wal, M. Bryjak, Y. Gogotsi, and P. M. Biesheuvel, *ACS Applied Materials & Interfaces* (2012).
16. J.-H. Lee, W.-S. Bae, and J.-H. Choi, *Desalination*, **258**, 159 (2010).
17. R. L. Clifton, C. A. Rios Perez, R. Naylor, and C. Hidrovo, in *10th International Conference on Nanochannels, Microchannels, and Minichannels*, p. 9, Rio Grande, Puerto Rico (2012).
18. E. Avraham, M. Noked, I. Cohen, A. Soffer, and D. Aurbach, *Journal of The Electrochemical Society*, **158**, P168 (2011).
19. Y. Bouhadana, E. Avraham, M. Noked, M. Ben-Tzion, A. Soffer, and D. Aurbach, *The Journal of Physical Chemistry C*, **115**, 16567 (2011).
20. R. F. Probstein, *Physicochemical Hydrodynamics*, John Wiley & Sons, Inc., Hoboken, New Jersey (2003).
21. R. S. Figliola and D. E. Beasley, *Theory and Design for Mechanical Measurements*, John Wiley & Sons, Inc., New York (2000).
22. F. P. Incropera, D. P. DeWitt, T. Bergman, and A. S. Lavine, *Fundamentals of heat and mass transfer*, Jhon Willey & Sons Inc., Hoboken, NJ (2007).
23. R. B. Bird, W. E. Stewart, and E. N. Lightfoot, *Transport Phenomena*, John Willey & Sons, Inc., New York (2007).
24. P. M. Biesheuvel, Y. Fu, and M. Z. Bazant, *Phys. Rev. E*, **83**, 061507 (2011).
25. P. M. Biesheuvel, R. Zhao, S. Porada, and A. van der Wal, *Journal of Colloid and Interface Science*, **360**, 239 (2011).
26. P. M. Biesheuvel and A. van der Wal, *Journal of Membrane Science*, **346**, 256 (2010).